PCCP

The CH($X^2\Pi$) + H2O Reaction: Two Transition State Kinetics

Journal:	*Physical Chemistry Chemical Physics*
Manuscript ID	CP-ART-05-2021-002234.R1
Article Type:	Paper
Date Submitted by the Author:	02-Jul-2021
Complete List of Authors:	Nguyen, Than Lam; University of Florida, Chemistry Peeters, Jozef; KU Leuven, Department of Chemistry

The CH($X^2\Pi$) + H_2O Reaction: Two Transition State Kinetics

Thanh Lam Nguyen[1]* and Jozef Peeters[2]

[1] *Quantum Theory Project, Department of Chemistry and Physics, University of Florida, Gainesville, FL. 32611, USA.*

[2]*Department of Chemistry, University of Leuven, Celestijnenlaan 200F, B-3001 Heverlee, Belgium.*

*Corresponding author: tlam.nguyen@chem.ufl.edu

Abstract

The reaction of ground state methylidyne (CH) with water vapor (H_2O) is theoretically re-investigated using high-level coupled cluster computations in combination with semi-classical transition state theory (SCTST) and two-dimensional master equation simulations. Insertion of CH into a H–O bond of H_2O over a submerged barrier via a well-skipping mechanism yielding solely H and CH_2O is characterized. The reaction kinetics is effectively determined by the formation of a pre-reaction van der Waals complex (PRC, HC—OH_2) and its subsequent isomerization to activated CH_2OH in competition with PRC re-dissociation. The tunneling effects are found to be minor, while variational effects in the PRC → CH_2OH step are negligible. The calculated rate coefficient $k(T)$ is nearly pressure-independent, but strongly depends on temperature with pronounced down-up behavior: a high value of 2×10^{-10} cm^3 s^{-1} at 50 K, followed by a fairly steep decrease down to 8×10^{-12} cm^3 s^{-1} at 900 K, but increasing again to 5×10^{-11} cm^3 s^{-1} at 3500 K. Over the T-range of this work, $k(T)$ can be expressed as:

$k(T, P=0) = 2.31\times10^{-11} (T/300\text{ K})^{-1.615} \exp(-38.45/T)$. cm^3 s^{-1} for T = 50 – 400 K

$k(T, P=0) = 1.15\times10^{-12} (T/300\text{ K})^{0.8637} \exp(892.6/T)$. cm^3 s^{-1} for T = 400 –1000 K

$k(T, P=0) = 4.57\times10^{-15} (T/300\text{ K})^{3.375} \exp(3477.4/T)$. cm^3 s^{-1} for T = 1000 –3500 K.

I. INTRODUCTION

Methylidyne (CH) is a highly reactive intermediate in the combustion of methane (CH_4) and other hydrocarbons.[1-4] Its high reactivity towards closed-shell molecules is owed in part to the vacant p-orbital on the C atom. CH in hydrocarbon flames has been shown to be responsible for the formation of chemi-ions by its reaction with O atoms[4] – the basis of the Flame Ionization Detector – and to be the source of prompt NO by its reaction with N_2,[5] while it was also identified as the source of chemi-luminescent OH by its reaction with O_2[6] – an important diagnostic tool in combustion studies. As water vapor (H_2O) is a principal product from combustion processes, CH can in principle react fairly fast with H_2O in a combustion environment, a reaction that could be a major loss process of CH in flames, in particular in fuel-rich conditions. Surprisingly, this reaction has not gained much attention; to the best of our knowledge, there are no reported experimental kinetics results at combustion temperatures. Both CH and H_2O have been detected in the interstellar medium,[7, 8] where the reaction between CH and H_2O can be expected to yield formaldehyde (CH_2O).[9]

$$CH(X^2\Pi) + H_2O = CH_2O + H \quad (1)$$

There are a number of experimental studies that have reported reaction rate constants over a temperature range between 50 K and 725;[9-12] all of these investigations found that the rate coefficient exhibits a negative temperature-dependence. The experimental results in the 300-725 K range can be divided in a set of lower rate constants and a set of higher rate constants, [9-12] the two sets differing by a factor of about 2.5.[9-12] The reason for this discrepancy is unclear, although the notorious difficulty to accurately establish or measure gas-phase H_2O concentrations could be a cause. Given that this reaction plays an important role in areas as diverse as combustion- and astrochemistry, further experimental studies as well as high-level theoretical calculations are warranted to resolve the above disagreement and to extend the temperature range for $k(T)$. There are several early quantum chemical and theoretical kinetics studies or interpretations,[9, 11, 13-15] which characterized a barrier-less insertion mechanism through a fairly stable pre-reactive complex (PRC), consistent with the experimental negative temperature-

dependence of the $k(T)$ rate coefficient.[9-12] Blitz et al.[10], relying in part on the quantum chemical result of Wang et al.[15] that the transition state for the actual insertion (TS1) is submerged for 6 kcal/mol, proposed that the reaction is controlled solely by the formation of the PRC; in their reasoning, the variational transition state (TS0) for formation of the PRC is very loose at low temperatures resulting in a high rate, whereas TS0 becomes gradually tighter at higher temperatures such that the rate decreases. Bergeat et al.[11] considered a two-transition state model, with TS0 and TS1 controlling the rate, and calculated the rate coefficient $k(T)$ using a master-equation technique.[11] They concluded that to fit the 'lower' experimental $k(T)$ set[10, 11] required a TS1 energy of −1.7 kcal/mol relative to the reactants, whereas the 'higher' $k(T)$ set required TS1 submerged for −3.9 kcal/mol, showing in any case that the energy of TS1 is an important quantity in co-determining the rate of the title reaction, even at moderately high temperatures.[11]

The first aim of this work is to use high-level coupled cluster calculations to construct the potential energy surface, focusing in particular on accurate energetics as well as vibration-rotation characteristics of TS1 which co-controls the rate already at moderate temperatures as shown by Bergeat et al.; [11] this will be combined with a proper variational treatment of TS0 for the barrier-less association entrance channel. Our second objective is to solve an *E,J*-resolved (two-dimensional) master equation in the frame of the two-TS model, in order to obtain rate constants as a function of both temperature and pressure. In this way we aim to provide highly accurate rate constants from first principles which can be compared with the experimental data and to extend the temperature range where $k(T)$ data are available to 3500 K for high-temperature combustion modeling involving the CH radical.

II. THEORETICAL METHODOLOGY

II.1. Coupled Cluster Quantum Chemical Calculations

All key stationary points on the lowest-lying doublet electronic potential energy surface for the reaction of CH and H_2O were fully optimized using a frozen core CCSD(T)/aug-cc-pVTZ level of theory.[16-18] Vibrational analyses were then done to confirm if the stationary points characterized are either a minimum (with all positive frequencies) or a transition state (with only one imaginary frequency that corresponds to the reaction coordinate). Anharmonic calculations were performed using the same level of theory to obtain anharmonic zero-point vibrational energy (ZPE), anharmonic constants, and ro-vibrational parameters for the following kinetics simulations. To obtain highly accurate relative energies, series of single-point energies with coupled cluster methods were then performed using a modification of the mHEAT-345(Q)[19] method reported recently (defined hereafter as amHEAT-345(Q)). Specifically, we have replaced cc-pVXZ basis sets[20] in the original mHEAT method by aug-cc-pVXZ basis sets[20] (where X = T, Q, and 5). Such a modification may be essential for chemical species having an unpaired electron and for long range interactions. The amHEAT-345(Q) is a composite method in which the energy is given as a sum of separately evaluated contributions:[19]

$$E_{mHEAT} = E^{\infty}_{SCF} + \Delta E^{\infty}_{CCSD(T)} + \Delta E_{T-(T)} + \Delta E_{(Q)-T} + \Delta E_{core} + \Delta E_{ZPE} + \Delta E_{DBOC} + \Delta E_{Scalar} + \Delta E_{SO} \qquad (2)$$

where E^{∞}_{SCF} is the Hartree-Fock energy extrapolated to a complete basis set (CBS) limit using aug-cc-pVXZ[20] (with X = T, Q, and 5) basis sets; $\Delta E^{\infty}_{CCSD(T)}$ is the electron correlation energy calculated in the frozen-core approximation with the CCSD(T) method[16-18] and extrapolated to a CBS limit using aug-cc-pVXZ (with X = Q and 5); $\Delta E_{T-(T)}$ is the energy difference of CCSDT and CCSD(T) calculations based on the cc-pVTZ basis set; $\Delta E_{(Q)-T}$ is the energy difference of CCSDT(Q)[21] and CCSDT calculations

using the cc-pVDZ basis set; ΔE_{core} is the core correlation correction; ΔE_{ZPE} is the anharmonic zero-point vibrational energy obtained in the framework of second-order vibration perturbation theory (VPT2);[22] ΔE_{DBOC} is the diagonal Born-Oppenheimer correction; ΔE_{Scalar} is the scalar relativistic effect; and ΔE_{SO} is the spin-orbit correction.

Further details of amHEAT have been documented elsewhere.[19] As seen in Figure 1, amHEAT calculations yield accuracies better than 0.2 kcal/mol as compared to benchmark ATcT values[23] for the reaction enthalpies; comparable accuracy can be expected for other species. Unless mentioned otherwise, all calculations were done using the CFOUR quantum chemistry package.[24, 25]

II.2. E,J-Resolved Master Equation Analysis

To be shown in next section, the chemical kinetics of the title reaction is effectively controlled by the formation step of pre-reactive complex (PRC), $HC^{\delta+}\text{—}^{-\delta}OH_2$, and its isomerization into CH_2OH. The most important portion of the potential energy surface (PES) that kinetically controls the reaction is given in Scheme 1.

$$CH + H_2O \underset{k_{PRC\rightarrow CH}(E,J)}{\overset{k_{CH\rightarrow PRC}(E,J)}{\rightleftharpoons}} PRC^* \xrightarrow{k_{PRC\rightarrow CH2OH}(E,J)} CH_2OH^* \xrightarrow{\text{Very fast}} CH_2O + H$$

Scheme 1: Effective chemical kinetics scheme for the title reaction.

An *E,J*-resolved two-dimensional master equation that describes the time evolution for the competition of decompositions of PRC and energy transfer processes through collisions of PRC with buffer gas is given by:[26-34]

$$\frac{\partial C_{PRC}(E_m,J_m)}{\partial t} = \sum_{J_n=0}^{J_{max}} \int_{E_n=0}^{E_{max}} P_{PRC}(E_m,J_m|E_n,J_n)\cdot\omega\cdot C_{PRC}(E_n,J_n)\cdot dE_n - \omega\cdot C_{PRC}(E_m,J_m) - \{k_{\mathrm{PRC}\rightarrow\mathrm{CH}}(E_m,J_m) + k_{\mathrm{PRC}\rightarrow H_2\mathrm{COH}}(E_m,J_m)\}\cdot C_{PRC}(E_m,J_m) + OST(E_m,J_m)$$

(3)

In Eq. 3, J_{max} is the maximum angular momentum; E_{max} is the maximum internal energy; $C_{PRC}(E_m,J_m,t)$ represents the (time-dependent) mole fractions of PRC in state (E_m,J_m) and time t; ω_{LJ} (in s^{-1}) is the Lennard-Jones collisional frequency;[35-37] and $k_{PRC\rightarrow H_2COH}(E_m,J_m)$ (in s^{-1}) is the (E_m,J_m)-resolved microcanonical rate coefficient for the isomerization step of PRC to CH_2OH. $P_{PRC}(E_m,J_m|E_n,J_n)$ is the *E,J*-resolved collisional transfer probability distribution function of PRC from state (E_n,J_n) to state (E_m, J_m). OST stands for the original source term, and is given by:[38-41]

$$OST(E_m,J_m) = F_{PRC}(E_m,J_m) \cdot k_{\infty}(T) \cdot [CH] \cdot [H_2O], \quad (4)$$

where $k_{\infty}(T)$ is the *capture rate constant* – that can be calculated using micro-variational transition state theory (μvTST)[42-45] (see Eq. 6 below) – for the barrier-less association step of CH and H_2O leading to PRC. $F_{PRC}(E_m,J_m)$ is the *E,J*-resolved initial distribution function for the nascent energized PRC and given by:[38, 41]

$$F_{PRC}(E_m,J_m) = \frac{(2J_m+1) \cdot k_{PRC\rightarrow CH}(E_m,J_m) \cdot \rho_{PRC}(E_m,J_m) \cdot \exp(-E_m/RT)}{\sum_{J_m=0}^{J_{max}}(2J_m+1)\int_{E_i=0}^{E_{max}} k_{PRC\rightarrow CH}(E_m,J_m) \cdot \rho_{PRC}(E_m,J_m) \cdot \exp(-E_m/RT) \cdot dE_m},$$

(5)

In Eq. 5, $\rho_{PRC}(E_m,J_m)$ is the density of ro-vibrational states for PRC, and $k_{PRC\rightarrow CH}(E_m,J_m)$ is the microcanonical rate constant for the PRC → CH + H_2O step, which is calculated using micro-variational TST.[45, 46]

$$k_{\infty}(T) = \frac{\sigma}{h} \times \frac{Q_{tr}^{\neq} Q_e^{\neq}}{Q_{CH}^{re} \cdot Q_{H_2O}^{re}} \times \sum_{J=0}^{\infty}(2J+1)\int_0^{\infty} Min[G_{rv}^{\neq}(E,J)] \times \exp\left(-E/k_BT\right)dE \quad (6)$$

where h is Planck's constant, k_B is Boltzmann's constant, and σ=2 is the reaction path degeneracy. T is the reaction temperature and E is the total internal energy. Min(G(E,J)) stands for minimizing the chemical reaction flux at each pair of *E* and *J*. Q_{CH}^{re} and $Q_{H_2O}^{re}$ are the complete partition functions for CH and H_2O, respectively, but without the symmetry number in the rotational partition function of H_2O. Q_{tr} is the translational partition function, and Q_e is the electronic partition function of the TS (the superscripts "re" and "≠" designate reactants and transition state (TS), respectively). Electronic partition functions for all stationary points are equal to 2 for a doublet electronic state. $G_{rv}^{\neq}$ is the sum of ro-vibrational quantum states of the TS for the given *E* and *J*, which can be obtained from its vibrational counterpart using the *J*-shifting approximation,[47-49] Eq. 7:

$$G_{rv}^{\neq}(E,J) = \sum_{K=-J}^{K=+J} G_v^{\neq}(E - E_r(J,K)) \quad (7a)$$

$$\rho_{rv}(E,J) = \sum_{K=-J}^{K=+J} \rho_v(E - E_r(J,K)) \quad (7b)$$

In Eq. 7, $G_v^{\neq}$ is the anharmonic (coupled) vibrational sum of states of TS that is calculated using Miller's semiclassical TST (SCTST) theory[50-54] on the basis of the Wang-Landau algorithm.[55-58] The SCTST theory[50-54] automatically includes coupled anharmonic vibrations and multi-dimensional quantum mechanical tunneling. E_r is the (external) rotational energy level of TS, which is approximated by a symmetric top,[59] Eq. 8:

$$E_r(J,K) = J(J+1)\overline{B} + (A - \overline{B})K^2, \text{ with } \overline{B} = \sqrt{B \cdot C} \text{ and } -J \le K \le +J \quad (8)$$

It is worthy to emphasize that for $CH(X^2\Pi)$ when T < 100 K in astronomical environments, there is a strong coupling of the 2D rotation and the electronic motion. Thus, the rotational energy values of the components of doublet states of CH were computed using Hill and Van Vleck's formalism.[60-62] The coupled rotational-electronic partition function of CH was then obtained through the direct state count, Eq. 9.

$$Q_{elec\_rot}^{CH}(T) = \sum_i n_i e^{-E_i/RT} \quad (9)$$

where n_i is the degeneracy number and E_i is the i^{th} eigenvalue.

All parameters (including collisional energy transfer, maximum energy, energy grain, and total angular momentum) used in the master-equation simulation are provided in Table S1 in the Supplementary Material. Given that the title reaction is only slightly pressure-dependent as shown in Fig. 3, the calculated rate coefficients in the pressure range of interest are only marginally influenced by the collisional parameters selected.

II.3. Variational Treatment for TS1

TS1 is a tight, well-defined transition state. As already mentioned above, Miller's SCTST theory is used to compute rate constants passing through TS1. However, it is well known that Miller's SCTST theory does not explicitly take variational effects into account. The variational effects are expected to reduce the chemical reaction flux via TS1, thus decreasing the overall rate constants. In this work, the variational effects are estimated by computing a ratio of rate constants with and without variational treatments, Eq. 10.

$$f_{ve}(T) = k_{with}(T)/k_{without}(T) \quad (10)$$

The variational treatment requires a minimum energy path along the reaction coordinate (RC) as well as ro-vibrational parameters of grid points on the RC.[63] In this work, the intrinsic reaction coordinate (IRC) was first computed using the UB97-1/6-311G(d,p)[64] level of theory. Harmonic vibrational frequency calculations with projecting out the RC[65] were then performed using the same UB97-1 level of theory to obtain ZPEs and ro-vibrational parameters for grid points on the RC. Relative energies were next refined using CCSD(T)/aug-cc-pVTZ single-point energy calculations based on the UB97-1 geometries (see Fig. S1 in the Supplementary Material).

From these data, both $k_{with}(T)$ and $k_{without}(T)$ can be computed at the low-pressure limit (LPL) using Eq. 11 (see below). Ratios ($f_{ve}(T)$) as a function of temperature (displayed in Fig. S2 in the Supplementary Material) show that the variational effects are found to be negligibly small, less than -2% for the entire temperature range considered in this work. The rationalization is that TS1 presents a sharp potential energy maximum (see Fig. S1), the imaginary frequency being i × 1503 cm^{-1}. So, in the results discussed below these variational effects are neglected.

III. RESULTS AND DISCUSSION

III.1. Potential Energy Surface (PES)

Figure 1 displays the important reaction pathways for the reaction between CH and H_2O. The first step is the barrier-less association leading to a pre-reactive complex (PRC), which has a binding energy of −8.93 kcal/mol. This PRC ($HC^{\delta+}$—$^{-\delta}OH_2$) is formed by a polar interaction of a lone pair orbital of the O atom and an empty p-orbital of the C atom. Subsequently, the PRC can isomerize to CH_2OH by insertion of CH into an O–H bond of H_2O through transition state TS1, in competition with re-dissociation of the PRC into the reactants. TS1 lies 1.43 kcal/mol below the initial reactants, such that the insertion of CH into H_2O is overall a barrier-less process. Important to note is the 1D hindered internal rotation (1DHR) of the H_a atom of the H_aOH_b moiety about the O–H_b axis, with H_b the shared atom (see Fig. 1); this results in a second, non-equivalent minimum at −1.16 kcal/mol, as shown in the hindered rotation PES as function of the rotation angle in Fig. S3. The quantum states of the 1DHR mode were found by solving the Schrödinger equation using the Multiwell program suite,[62] and its integrated sum of states $G_v(E)$ was convoluted with the anharmonic (coupled) vibrational sum of accessible states of the other modes. The CH_2OH* produced has a high vibrational excitation energy of about 87 kcal/mol, thus quickly decaying to H + CH_2O via H-loss. The H-elimination to yield H + CH_2O can occur directly via TS4 or indirectly after conversion to CH_3O. All three barriers of TS2, TS3, and TS4 lie very low in energy as compared to the

available internal energy of CH_2OH^*, so CH_2OH^* and CH_3O^* are highly unlikely to be thermalized by collisions unless at very high pressures of >100 atm. As a result, the roles of the intermediates CH_2OH/CH_3O are kinetically unimportant; such a mechanism is known as well-skipping. CH_2OH^* might decompose via TS5 for H_2-loss leading to H_2 + HOC, but this pathway must overcome a high barrier of 83.5 kcal/mol and is therefore negligible and irrelevant.

III.2. Reaction Rate Coefficients

As explained above, the mechanism and kinetics of the title reaction are effectively governed by the initial step of CH + H_2O → PRC ($HC^{\delta+}$—$^{-\delta}OH_2$) through the variational entrance TS0 and PRC isomerization through TS1 to yield CH_2OH^* (see Figure 1) in competition with PRC re-dissociation through TS0, a prototype of the 2-TS kinetics model.[66-68] It is fairly well established[10] that formation of the PRC through the loose, variational TS0, governed by the long-range interaction between CH and H_2O, limits the reaction kinetics at low to moderate temperatures, while the isomerization of PRC over the submerged TS1 — with its higher total number of accessible ro-vibration states — far outruns re-dissociation of the PRC through TS0. So, a proper variational treatment of the bottleneck TS0 is desired to obtain highly accurate rate constants. For the tight inner TS1, Miller's SCTST theory is used to compute $k_{PRC\rightarrow CH2OH}(E,J)$, while microvariational TST theory is used to locate the kinetic bottleneck TS0 and to obtain $k_{CH\leftrightarrow PRC}(E,J)$ by minimizing the chemical reaction flux. Figure 2 presents the minimum-energy path for the barrier-less association of CH and H_2O yielding the PRC, constructed using CCSD(T)/aug-cc-pV5Z calculations based on the CCSD(T)/aug-cc-pVTZ geometry. In addition, the electron correlation corrections from fully triple electron excitations (with CCSDT/cc-pVTZ) and non-iterative quadruple electron excitations (with CCSDT(Q)/cc-pVDZ) were also included. A temperature of 50 K was chosen as lower limit for the microvariational treatment of TS0, because at even lower temperatures the interaction between CH and H_2O is very long-range, such that TS0 becomes too loose to be described by a rigid-rotor, harmonic oscillator model. Calculation of the tunneling factor, which is

always small, < 1.5, is incorporated in the SCTST implementation. The $k(T,P)$ results described below were not corrected for the very small variational effect (see Methodologies section), which is always less than 2% (see Fig. S2).

Figure 3 shows fall-off curves for $k(T,P)$ for T = 50 to 1000 K and P = 1 to 10^6 Torr, obtained by solving the *E,J*-resolved master equation (3). As seen, the reaction is marginally pressure-dependent up to about 1 atm, on account of the short lifetime of the PRC complex, about 0.1 ns, due to the fast PRC → CH_2OH* step. The difference between 1 Torr to 1000 Torr is found to be less than 5%. It is therefore concluded that the reaction is practically in the low-pressure limit where an *exact* solution of the two-dimensional master equation can be obtained, as given by:[69, 70]

$$k_{LPL}(T,P=0) = \frac{\sigma}{h} \times \frac{Q_{tr}^{\neq} Q_{e}^{\neq}}{Q_{CH}^{re} \cdot Q_{H_2O}^{re}} \times \sum_{J=0}^{\infty} (2J+1) \int_{0}^{\infty} \frac{Min\left(G_0^{\neq}(E,J)\right) \times G_1^{\neq}(E,J)}{Min\left(G_0^{\neq}(E,J)\right) + G_1^{\neq}(E,J)} \times \exp\left(-E/k_B T\right) dE \quad (11)$$

where $Min\left(G_0^{\neq}(E,J)\right)$ stands for the minimum value of the sum of ro-vibration states $G_0^{\neq}(E,J)$ for the variational TS0 along the reaction path for given *E,J*, and $G_1^{\neq}(E,J)$ is the sum of ro-vibrational states of TS1 for given *E,J*.e

However, the reaction strongly depends on temperature; and is found to exhibit negative temperature-dependence up to about 900 K, thus being consistent with the experimental data.[9-12] Figure 4 shows the calculated rate coefficient, using eq. (11), not corrected for the negligible variational effect of TS1, for a wide temperature range between 50 K and 3500 K, which covers most practical applications from chemistry in interstellar clouds to combustion. Figure 4 shows that the negative temperature dependence of the rate coefficient holds up only to about 900 K, where $k(T, P=0)$ reaches a minimum, above which it increases markedly with temperature. This new finding has important implications for the combustion chemistry of the CH radical. This behavior is explained as follows — referring also to Fig. S4 which shows additionally the hypothetical $k(T, P=0)$ if solely TS1 were to limit the reaction rate at all T ,

i.e. if TS0 were to possess an infinite number of ro-vibration states. In the low-to-moderate temperature regime, the forward chemical reactive flux to the PRC via the loose, variational, outer TS0 is the rate-determining step, such that the rate coefficient decreases with temperature as TS0 becomes more rigid at higher temperature. Starting from about 300 K, TS1 begins to take some control of the reaction together with TS0, i.e. part of the PRC re-dissociates, further depressing the reaction rate; the reason for this is the higher rigidity of TS1 compared to TS0. At about 900 K, $k(T)$ bottoms out and above 1000 K, the more rigid TS1 becomes the sole rate-limiting transition state, while at the same time $k(T)$ increases again with temperature, because once T > 1000 K, the 1DHR mode with its closely spaced lower eigenvalues (see Fig. S3), the bending vibration modes and the C–O stretch of TS1 are or become activated, increasing the partition function Q of TS1 faster than that of the reactants with only one bending mode and 5 relative rotation and translation modes for which Q increases only as $T^{5/2}$.

Figure 4 shows that the calculated rate constants support the high experimental values of $k(T)$ of $(2 – 0.3) \times 10^{-10}$ cm^3 s^{-1} in the 50 – 300 K range observed by Hickson et al.[9], although our values are on average 2 times lower. In addition, the values from first principles are a constant factor of *ca.* 1.5 higher that the experimental results of Blitz et al.[10] and that of Bergeat et al.[11]: $k_{exp}(T) = 2 \times 10^{-11} – 5 \times 10^{-12}$ cm^3 s^{-1} in the 300–725 K range, but are about 2 times lower than the data of Zabarnick et al.[12] in the same range. As noted by Bergeat et al.,[11] the $k(T)$ values in this range depend markedly on the precise energy of the submerged TS1; our accurate high-level *ab initio* results put this energy at a high −1.43 kcal/mol and therefore favor the lower k values. Also, the present theoretical data show a smoother transition from the low-T to the moderate-T regimes than the experimental results. The sets of experimental data on the whole suggest that further experimental studies are warranted. Further theoretical work that focuses on the kinetics at very low temperatures could examine the merits of variable reaction coordinate TST[71] for an alternative description of the loose TS0.

For the purpose of modelling, the first-principles $k(T)$ of this work over the 50 – 3500 K range can be expressed as:

$k(T, P=0) = 2.31\times10^{-11}\ (T/300\ \mathrm{K})^{-1.615}\ \exp(-38.45/T)$. $\mathrm{cm^3\ s^{-1}}$ for $T = 50 - 400$ K

$k(T, P=0) = 1.15\times10^{-12}\ (T/300\ \mathrm{K})^{0.8637}\ \exp(892.6/T)$. $\mathrm{cm^3\ s^{-1}}$ for $T = 400$ -–1000 K

$k(T, P=0) = 4.57\times10^{-15}\ (T/300\ \mathrm{K})^{3.375}\ \exp(3477.4/T)$. $\mathrm{cm^3\ s^{-1}}$ for $T = 1000$ -3500 K

In addition, the calculated rate constants from first-principles are also provided in Table S2 in the Supplementary Material.

IV. CONCLUSIONS

In this work, high-level coupled cluster calculations were used to characterize the rate determining steps for the reaction of methylidyne and water vapor, of interest to combustion chemistry and chemistry in the interstellar medium. The barrier-less insertion of CH into H_2O is confirmed to proceed via a well-skipping mechanism *directly* yielding H and CH_2O exclusively. Of the two controlling transition states, the loose entrance bottleneck, TS0, is characterized by a proper variational treatment while the inner, tight, submerged TS1 is characterized at high levels of theory. TS0 is confirmed to uniquely determine the reaction rate at low temperatures, though only up to *ca.* 300 K. TS1 is found to lie at –1.43 kcal/mol, substantially higher in energy that in previous theoretical studies, such that TS1 begins to influence the reaction rate already at T *ca.* 300 K, and takes full control of the reaction rate once $T \geq$ 1000, The rate coefficient $k(T)$, calculated using a two-dimensional master equation technique for extended temperature and pressure ranges (T=50–3500 K and P=1–10^6 Torr) is found to be nearly pressure-independent, but strongly dependent on temperature, showing a down-up behavior with increasing T. At T = 50 K, as in interstellar clouds, the theoretical $k(T)$ is *ca.* 2×10^{-10} $\mathrm{cm^3\ s^{-1}}$, in agreement with a recent experimental value.[9] At increasing temperatures, the $k(T)$ of this work first decreases markedly, favoring the lower available experimental values in the 300 – 725 K range. We provide the first kinetics data on this reaction for T> 725 K: the first-principles $k(T)$ bottoms out at 900 K

with a value of 8×10^{-12} cm^3 s^{-1} and further increases again to reach 5×10^{-11} cm^3 s^{-1} at 3500 K. It is therefore concluded that the reaction is an important if not major CH removal process in hydrocarbon combustion.

Supplementary Material

See the supplementary material for optimized geometries, ro-vibrational parameters, anharmonic constants, the calculated rate coefficients, and additional figures.

Acknowledgments

TLN would like to thank the Department of Chemistry, University of Florida for financial support. TLN wishes to thank Prof. John F. Stanton (UF) for his support, encouragement, and helpful advices. This material is based on work partly supported by the U.S. Department of Energy, Office of Basic Energy Sciences under Award DE-SC0018164. JP is grateful to the University of Leuven for continued support, even on turning 80.

DATA AVAILABILITY

The data that support the findings of this study are available within the article and its supplementary material. The data that support the findings of this study are available from the corresponding author upon reasonable request.

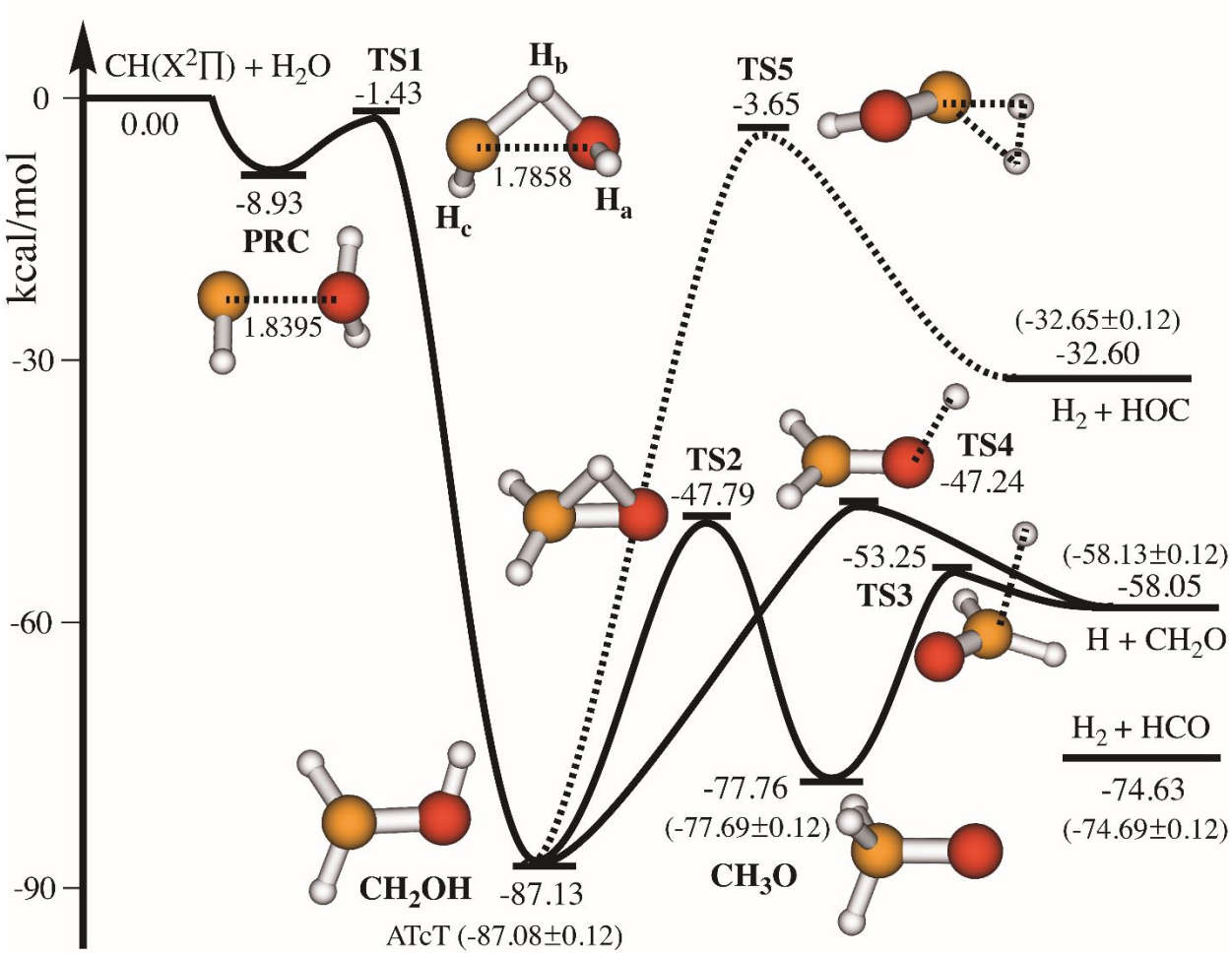

Figure 1: Schematic reaction energy profile for the reaction of $CH(X^2\Pi) + H_2O$ constructed using the amHEAT-345(Q) method (see text). Benchmark ATcT[23] values are also given in parentheses for comparison.

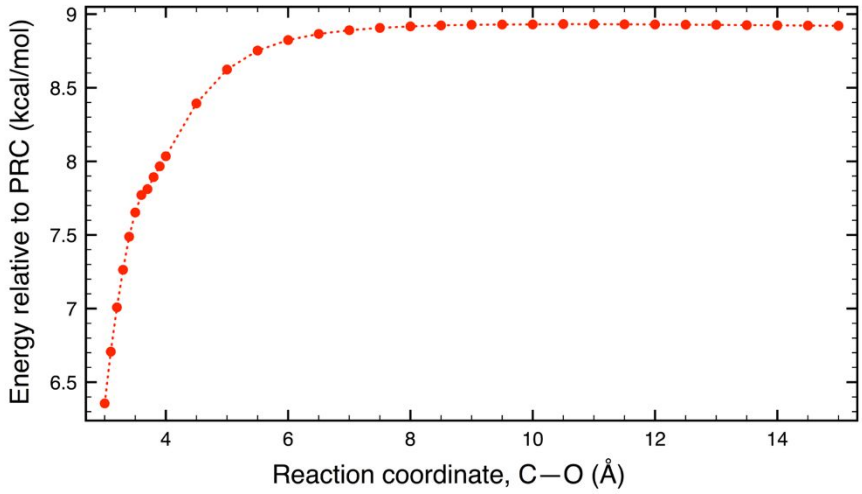

Figure 2: Minimum energy path for the association of CH($X^2\Pi$) and H_2O leading to pre-reactive complex, PRC, calculated using the CCSD(T)/aug-cc-pV5Z + ZPE + $\Delta E_{T-(T)}$ + $\Delta E_{(Q)-T}$ level of theory (see text).

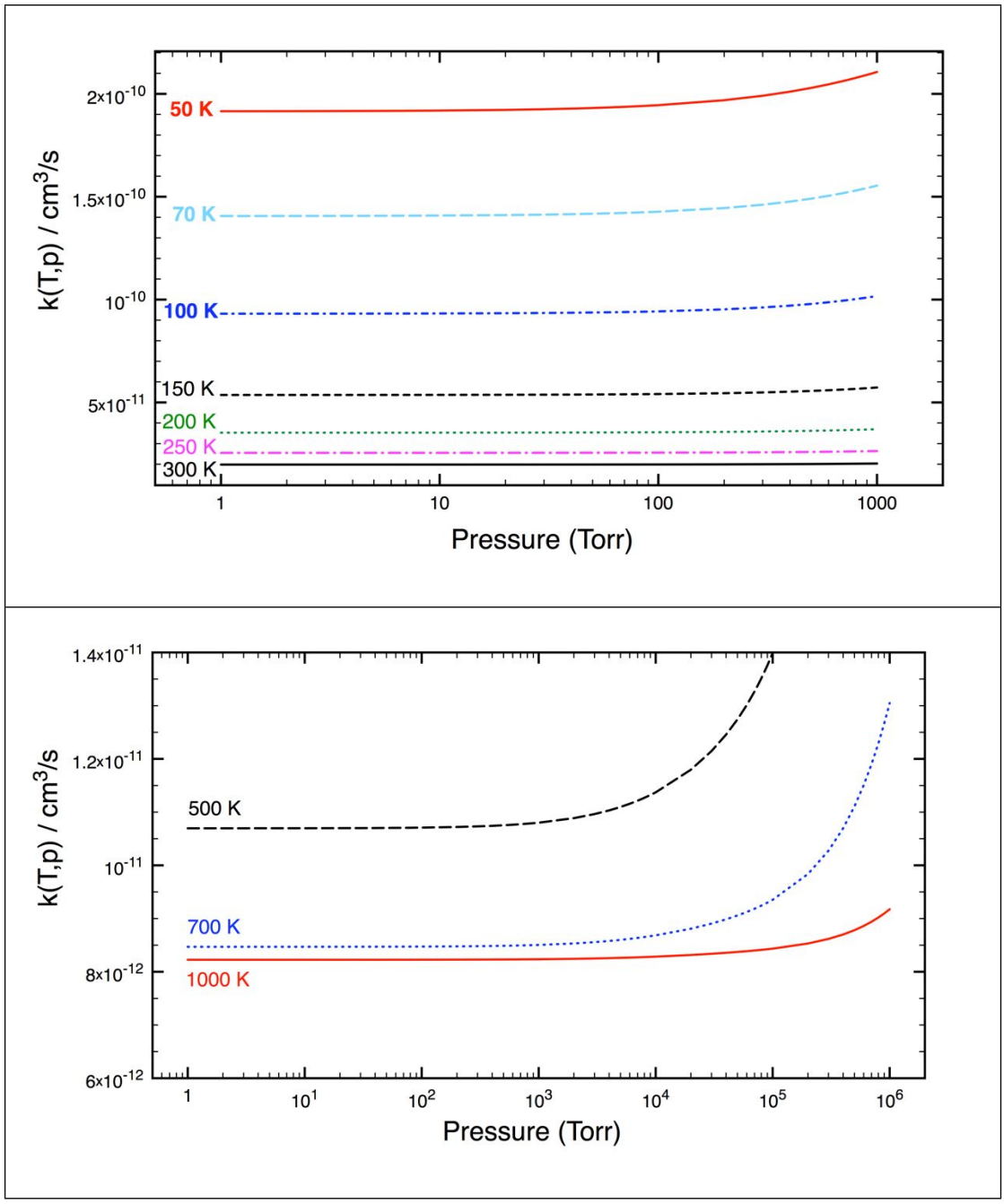

Figure 3: Fall-off curves for the CH($X^2\Pi$) + H_2O reaction calculated for an extensive range of temperature (T=50–1000 K) and pressure (P=1–10^6 Torr). Note that when T > 1000 K, the reaction becomes effectively pressure-independent.

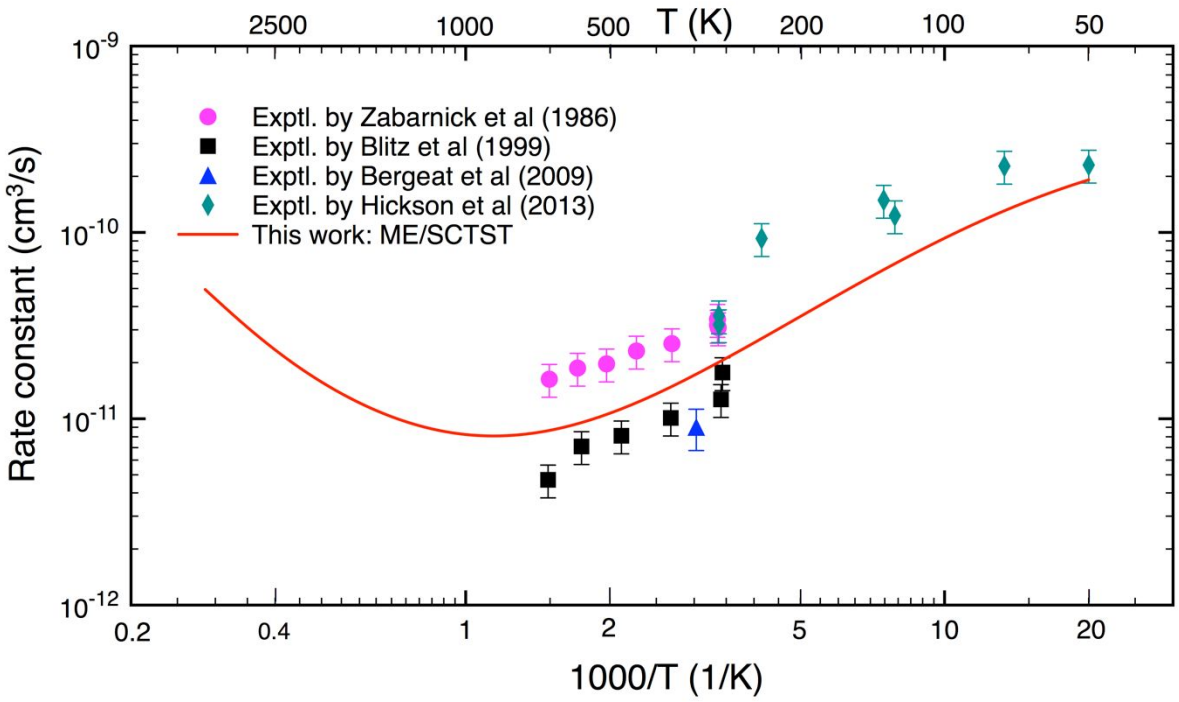

Figure 4: Rate coefficients for the CH($X^2\Pi$) + H_2O reaction calculated for an extensive temperature range between 50 K and 3500 K. Experimental data[9-12] are included for comparison.

References

1. W. C. Gardiner, *Gas-phase combustion chemistry*, Springer, New York, 2000.
2. D. L. Baulch, C. T. Bowman, C. J. Cobos, R. A. Cox, T. Just, J. A. Kerr, M. J. Pilling, D. Stocker, J. Troe, W. Tsang, R. W. Walker and J. Warnatz, *J Phys Chem Ref Data*, 2005, **34**, 757-1397.
3. J. A. Miller, M. J. Pilling and E. Troe, *Proc Combust Inst*, 2005, **30**, 43-88.
4. J. Peeters and C. Vinckier, *Proc Combust Inst*, 1975, **15**, 969-977.
5. J. Blauwens, B. Smets and J. Peeters, *Proc. Combust. Inst.* , 1977, **16**, 1055-1064.
6. S. A. Carl, M. Van Poppel and J. Peeters, *J Phys Chem A*, 2003, **107**, 11001-11007.
7. I. R. Cooke and I. R. Sims, *Acs Earth Space Chem*, 2019, **3**, 1109-1134.
8. D. McElroy, C. Walsh, A. J. Markwick, M. A. Cordiner, K. Smith and T. J. Millar, *Astron Astrophys*, 2013, **550**.
9. K. M. Hickson, P. Caubet and J. C. Loison, *J Phys Chem Lett*, 2013, **4**, 2843-2846.
10. M. A. Blitz, M. Pesa, M. J. Pilling and P. W. Seakins, *J Phys Chem A*, 1999, **103**, 5699-5704.
11. A. Bergeat, S. Moisan, R. Mereau and J. C. Loison, *Chem Phys Lett*, 2009, **480**, 21-25.
12. S. Zabarnick, J. W. Fleming and M. C. Lin, *J Chem Phys*, 1986, **85**, 4373-4376.
13. B. S. Jursic, *J Phys Chem A*, 1998, **102**, 9255-9260.
14. E. Mazarei and S. H. Mousavipour, *J Phys Chem A*, 2017, **121**, 8033-8047.
15. Z. X. Wang, R. Z. Liu, M. B. Huang and Z. H. Yu, *Can J Chem*, 1996, **74**, 910-917.
16. K. Raghavachari, G. W. Trucks, J. A. Pople and M. Headgordon, *Chem Phys Lett*, 1989, **157**, 479-483.
17. R. J. Bartlett, J. D. Watts, S. A. Kucharski and J. Noga, *Chem Phys Lett*, 1990, **165**, 513-522.
18. J. F. Stanton, *Chem Phys Lett*, 1997, **281**, 130-134.
19. J. H. Thorpe, C. A. Lopez, T. L. Nguyen, J. H. Baraban, D. H. Bross, B. Ruscic and J. F. Stanton, *J Chem Phys*, 2019, **150**.
20. T. H. Dunning, *J Chem Phys*, 1989, **90**, 1007-1023.
21. M. Kalley and et. al. MRCC, a quantum chemical program suite written by M. Kallay, et. al. See J. Chem. Phys. 139, 094105 (2013), as well as: www.mrcc.hu.

22. I. M. Mills, Vibration-Rotation Structure in Asymmetric- and Symmetric-Top Molecules. In Molecular Spectroscopy: Modern Research; Rao, K. N.; Mathews, C. W., Ed.; Academic Press: New York. **1972,** *Vol. 1*, 115.

23. B. Ruscic and D. H. Bross, Active Thermochemical Tables (ATcT) values based on ver. 1.122f of the Thermochemical Network (2021), available at ATcT.anl.gov).
24. J. F. Stanton and et. al., CFOUR, a quantum chemical program package. *For the current version, see http://www.cfour.de*.
25. D. A. Matthews, L. Cheng, M. E. Harding, F. Lipparini, S. Stopkowicz, T. C. Jagau, P. G. Szalay, J. Gauss and J. F. Stanton, *J Chem Phys*, 2020, **152**.
26. S. J. Jeffery, K. E. Gates and S. C. Smith, *J. Phys. Chem.*, 1996, **100**, 7090-7096.
27. S. H. Robertson, M. J. Pilling and N. J. B. Green, *Mol Phys*, 1996, **89**, 1531-1551.
28. J. A. Miller, S. J. Klippenstein and C. Raffy, *J. Phys. Chem.*, 2002, **106**, 4904-4913.
29. A. W. Jasper, K. M. Pelzer, J. A. Miller, E. Kamarchik, L. B. Harding and S. J. Klippenstein, *Science*, 2014, **346**, 1212-1215.
30. P. K. Venkatesh, A. M. Dean, M. H. Cohen and R. W. Carr, *J. Chem. Phys.*, 1999, **111**, 8313-8329.
31. T. L. Nguyen and J. F. Stanton, *The Journal of Physical Chemistry A*, 2020, DOI: https://pubs.acs.org/doi/10.1021/acs.jpca.9b11379.
32. T. L. Nguyen and J. F. Stanton, *J Phys Chem A*, 2015, **119**, 7627-7636.
33. T. L. Nguyen, H. Lee, D. A. Matthews, M. C. McCarthy and J. F. Stanton, *J Phys Chem A*, 2015, **119**, 5524-5533.
34. T. L. Nguyen and J. F. Stanton, *J Phys Chem A*, 2018, **122**, 7757-7767.
35. J. Troe, *J Chem Phys*, 1977, **66**, 4745-4757.
36. R. C. Reid, J. M. Prausnitz and T. K. Sherwood, *The Properties of Gases and Liquids*, 1977.
37. P. D. Neufeld, R. A. Aziz and A. R. Janzen, *J Chem Phys*, 1972, **57**, 1100-&.

38. K. A. Holbrook, M. J. Pilling, S. H. Robertson and P. J. Robinson, *Unimolecular reactions*, Wiley, Chichester ; New York, 2nd edn., 1996.
39. R. G. Gilbert and S. C. Smith, *Theory of unimolecular and recombination reactions*, Blackwell Scientific Publications ; Publishers' Business Services distributor, Oxford ; Boston Brookline Village, Mass., 1990.
40. W. Forst, *J Chem Phys*, 1968, **48**, 3665-&.
41. W. Forst, *Unimolecular reactions : a concise introduction*, Cambridge University Press, Cambridge, U.K. ; New York, 2003.
42. H. Eyring, *J Chem Phys*, 1935, **3**, 107-115.
43. M. G. Evans and M. Polanyi, *T Faraday Soc*, 1935, **31**, 0875-0893.
44. D. G. Truhlar, B. C. Garrett and S. J. Klippenstein, *J Phys Chem-Us*, 1996, **100**, 12771-12800.
45. W. L. Hase, *Accounts Chem Res*, 1983, **16**, 258-264.
46. D. G. Truhlar and B. C. Garrett, *Annu Rev Phys Chem*, 1984, **35**, 159-189.
47. W. H. Miller, *J Am Chem Soc*, 1979, **101**, 6810-6814.
48. J. M. Bowman, *J Phys Chem-Us*, 1991, **95**, 4960-4968.
49. N. Balakrishnan, *J Chem Phys*, 2003, **119**, 195-199.
50. W. H. Miller, *Faraday Discuss*, 1977, **62**, 40-46.
51. W. H. Miller, R. Hernandez, N. C. Handy, D. Jayatilaka and A. Willetts, *Chem Phys Lett*, 1990, **172**, 62-68.
52. R. Hernandez and W. H. Miller, *Chem Phys Lett*, 1993, **214**, 129-136.
53. T. L. Nguyen, J. F. Stanton and J. R. Barker, *Chem Phys Lett*, 2010, **499**, 9-15.
54. T. L. Nguyen, J. F. Stanton and J. R. Barker, *J Phys Chem A*, 2011, **115**, 5118-5126.
55. F. G. Wang and D. P. Landau, *Phys Rev Lett*, 2001, **86**, 2050-2053.
56. F. G. Wang and D. P. Landau, *Phys Rev E*, 2001, **64**.
57. M. Basire, P. Parneix and F. Calvo, *J Chem Phys*, 2008, **129**.
58. T. L. Nguyen and J. R. Barker, *J Phys Chem A*, 2010, **114**, 3718-3730.
59. T. Baer and W. L. Hase, *Unimolecular reaction dynamics : theory and experiments*, Oxford University Press, New York, 1996.
60. E. Hill and J. H. Van Vleck, *Phys Rev*, 1928, **32**, 0250-0272.
61. T. L. Nguyen, B. Ruscic and J. F. Stanton, *J Chem Phys*, 2019, **150**.
62. J. R. Barker, T. L. Nguyen, J. F. Stanton, C. Aieta, M. Ceotto, F. Gabas, T. J. D. Kumar, C. G. L. Li, L. L. Lohr, A. Maranzana, N. F. Ortiz, J. M. Preses, J. M. Simmie, J. A. Sonk and P. J. Stimac. *MULTIWELL Program Suite*, Climate and Space Sciences and Engineering, University of Michigan, Ann Arbor, MI 48109-2143. Jan. 2021.
63. D. G. Truhlar and et. al., POLYRATE 2015: Computer Program for the Calculation of Chemical Reaction Rates for Polyatomics. **2015**.
64. F. A. Hamprecht, A. J. Cohen, D. J. Tozer and N. C. Handy, *J Chem Phys*, 1998, **109**, 6264-6271.
65. A. G. Baboul and H. B. Schlegel, *J Chem Phys*, 1997, **107**, 9413-9417.
66. E. E. Greenwald, S. W. North, Y. Georgievskii and S. J. Klippenstein, *J Phys Chem A*, 2005, **109**, 6031-6044.
67. T. L. Nguyen and J. F. Stanton, *J Phys Chem A*, 2013, **117**, 2678-2686.
68. T. L. Nguyen and J. F. Stanton, *J Phys Chem Lett*, 2020, **11**, 3712-3717.
69. T. L. Nguyen, B. C. Xue, R. E. Weston, J. R. Barker and J. F. Stanton, *J Phys Chem Lett*, 2012, **3**, 1549-1553.
70. J. Troe, *J Chem Soc Faraday T*, 1994, **90**, 2303-2317.
71. L. B. Harding, Y. Georgievskii and S. J. Klippenstein, *J Phys Chem A*, 2005, **109**, 4646-4656.